Received: 22 July 2025 | Accepted: 29 December 2025

DOI: 10.1002/bmm2.70079

RESEARCH ARTICLE

BMEMat WILEY

Real time in vivo efficacy monitoring of desialylation and perforation enhanced immunotherapy of cancer

Yuanjiao Yang[1,2] | Yuru Wang[1] | Xuemei Li[3] | Chaoyi Yang[1] | Yuhui Yang[1] | Yanyun Fang[1] | Lin Ding[1] | Yunlong Chen[1] | Huangxian Ju[1]

[1]State Key Laboratory of Analytical Chemistry for Life Science, School of Chemistry and Chemical Engineering, Nanjing University, Nanjing, China

[2]The First Affiliated Hospital of USTC, Division of Life Sciences and Medicine, University of Science and Technology of China, Hefei, China

[3]Shandong Province Key Laboratory of Detection Technology for Tumor Markers, School of Chemistry and Chemical Engineering, Linyi University, Linyi, China

Correspondence
Yunlong Chen and Huangxian Ju.
Email: ylc@nju.edu.cn and hxju@nju.edu.cn

Funding information
National Natural Science Foundation of China, Grant/Award Numbers: 22474057, 82503538; The program B for Outstanding PhD candidate of Nanjing University

Abstract

Efficient enhanced NK cell therapy is of critical importance in the immune treatment of cancer. Real time monitoring provides the necessary means for precise treatment and improving its efficacy. This work designed a powerful nanomedicine (MFMAF-7) to engineer NK cells for perforation and desialylation by encapsulating streptolysin O conjugated neuraminidase, adenosine-triphosphate (ATP)-responsive DNA and granzyme B (GrB)-responsive peptide (SLO-NEU, SLO-AD, SLO-GP) in cholesterol and aptamer-modified zeolitic metal azolate framework-7. After targeted delivery of the engineered NK cells to tumor region, the nanomedicine is degraded to release SLO-NEU, SLO-AD and SLO-GP, which then perforate tumor cells to promote the delivery of cytokines. The anchored SLO-NEU can cleave sialic acids for inhibiting the immune evasion of tumor cells and activating the NK cells to release cytokines, while the SLO-AD and SLO-GP can in situ visualize the levels of both ATP and GrB for assessing the efficacy in real time. The in vivo experiments with tumor-bearing mice demonstrate the enhanced efficacy of immunotherapy and the feasibility of real time monitoring with the proposed nanomedicine.

KEYWORDS

enhanced immunotherapy, nanomedicine, NK cell, perforation and desialylation, real-time monitoring

1 | INTRODUCTION

Natural killer (NK) cell therapy utilizes the innate immune-killing and strong cytolytic ability of NK cells to attack tumor cells without damage to healthy cells,[1–4] and has become one of the most promising clinical strategies to treat and cure cancer. To trick the immune system to evade immune-killing, tumor cells smartly evolve to reduce the intrinsic immunogenicity by over-expressing sialylated ligands, which bind the inhibitory

Yuanjiao Yang and Yuru Wang contributed equally.

receptors sialic acid (SA)-binding Ig-like lectins (Siglecs),[5] on NK cells to suppress the immune response and initiate immune evasion.[4–10] In addition, SA on tumor cells can also disturb the interaction of NK-activating receptors natural killer group 2D (NKG2D) with its ligands to inhibit NK activation.[7] Therefore, desialylation of tumor cells can simultaneously decrease the binding of Siglecs to inhibit immune evasion and increase the binding of NKG2D to promote the activation of NK cells for enhanced NK cell therapy. On the other hand, the delivery of the cytokines released from NK cells is also critical to the efficiency of the NK cell therapy.[11] Once NK cells are activated, the released cytotoxic granules or cytokines, such as granzyme B (GrB), must be delivered into the tumor cells to induce their apoptosis or modulate the immune system for further immune-killing.[11–13] Thus, the assistance of perforation for the delivery is another efficient method to enhance the efficacy of NK cell therapy. Moreover, in vivo detection of GrB level can be used for the real time monitoring of immunotherapy efficacy.

According to the functions of SA during the immune-killing process, many methods have been developed to enhance the immunotherapeutic efficacy by SA-blockage,[14] SA-inhibition,[15] or SA-cleavage.[4, 15–17] After bacterial pore-forming exotoxin streptolysin O (SLO)[18] is conjugated to different functional molecules, such as neuraminidase (NEU) and galactose, these molecules can be modified on cell surface by the perforating activity of SLO to perform SA-cleavage, activate immune cells or deliver cytokines for immune-killing of the modified cells.[12, 17, 18] Despite of the efficient enhancement of immunotherapy achieved by individual or simultaneous utilization of the desialylation and perforation strategies, the lacks of immune cells and in vivo monitoring methods still essentially limited the further improvement of immunotherapy efficacy.

Recently, the engineering of extrinsic NK cells with targeting functions,[19] such as chimeric antigen receptors (CARs),[20] antibody-cell-conjugations (ACCs),[21] glycans[22] and aptamers,[23] has attracted considerable attention in improving immunotherapy efficacy. Current clinical NK therapies, such as CAR-NK cells and antibody-conjugated NK cells, primarily focus on enhancing tumor recognition and targeting specificity, but elide on the immune evasion caused by the hyper-sialylated tumor microenvironment and inefficient penetration of the cytotoxic granules into tumor cells.

Here we design a powerful nanomedicine, multi-functional zeolitic metal azolate framework-7 (MFMAF-7), to engineer the NK cells by encapsulating three different kinds of SLO conjugates, SLO-NEU, SLO-adenosinetriphosphate (ATP)-responsive DNA (SLO-AD) and SLO-GrB-responsive peptide (SLO-GP), in cholesterol and aptamer-modified zeolitic metal azolate framework-7 (MAF-7) (Figure 1a). Through the cholesterol mediated embedding,[16] the nanomedicine endows the NK cells with not only the enhanced immunotherapy efficacy through perforation and desialylation but also real time in vivo efficacy monitoring capability (Figure 1b). After i.v. injection into the tumor-bearing mice, the MFMAF-7 engineered NK cells can be delivered to the tumor region by tumor-targeting aptamer (Apt).[24] In an acidic microenvironment,[25] the pH-responsive MAF-7[26] is degraded to release SLO-NEU, SLO-AD, and SLO-GP and anchor NEU, AD and GP on tumor cells. NEU - mediated desialylation and SLO mediated perforation efficiently enhance the NK cell therapy by the inhibition of immune evasion, promotion of NK cell activation, and assisting perforation. More importantly, the GrB released from NK cells can remove the Texas red (TR) fluorescence quencher (BHQ2) in SLO-GP to recover the fluorescence of TR, while the ATP released from the dying tumor cells is bound by the clip structure of AD to quench the fluorescence of Cy5.5 by the corresponding quencher BHQ3, which achieves real time in vivo efficacy monitoring of the immune-killing process[27–30] and the death situation of tumor cells.[31, 32]

As a proof of concept, the 4T1 tumor-bearing mice were used as models to demonstrate the perforation and desialylation enhanced NK cell therapy of tumors and real time in vivo efficacy monitoring, providing a promising therapy and efficacy monitoring strategy for the clinical therapy of cancer.

2 | RESULTS AND DISCUSSION

2.1 | Characterization and functions of SLO conjugates

SLO-NEU was prepared by conjugating azide modified α2-3,6,8 neuraminidase A (NEU-N_3) to dibenzocyclooctyne modified SLO (SLO-DBCO).[17, 33] SLO-AD was prepared with three functional DNA sequences AD1, AD2 and AD3 according to a previous report.[31] AD1 was terminated with Cy5.5 and BHQ3, while AD2 and AD3 contained the recognizing sequences for ATP. SLO-GP was synthesized by reacting TR labeled GrB-responsive peptide 1 (GP1-TR) with SLO and then BHQ2-NHS. Compared to SLO, the m/z values of SLO-AD and SLO-GP respectively varied from 60 KDa to 139 KDa and 66 KDa (Figure S1a,b) with the differently distributed band positions in the SDS-PAGE gel (Figure S1e), indicating the successful conjugation of NEU, AD and GP to SLO. The functions of SLO-AD and SLO-GP were investigated by an in vitro fluorescence

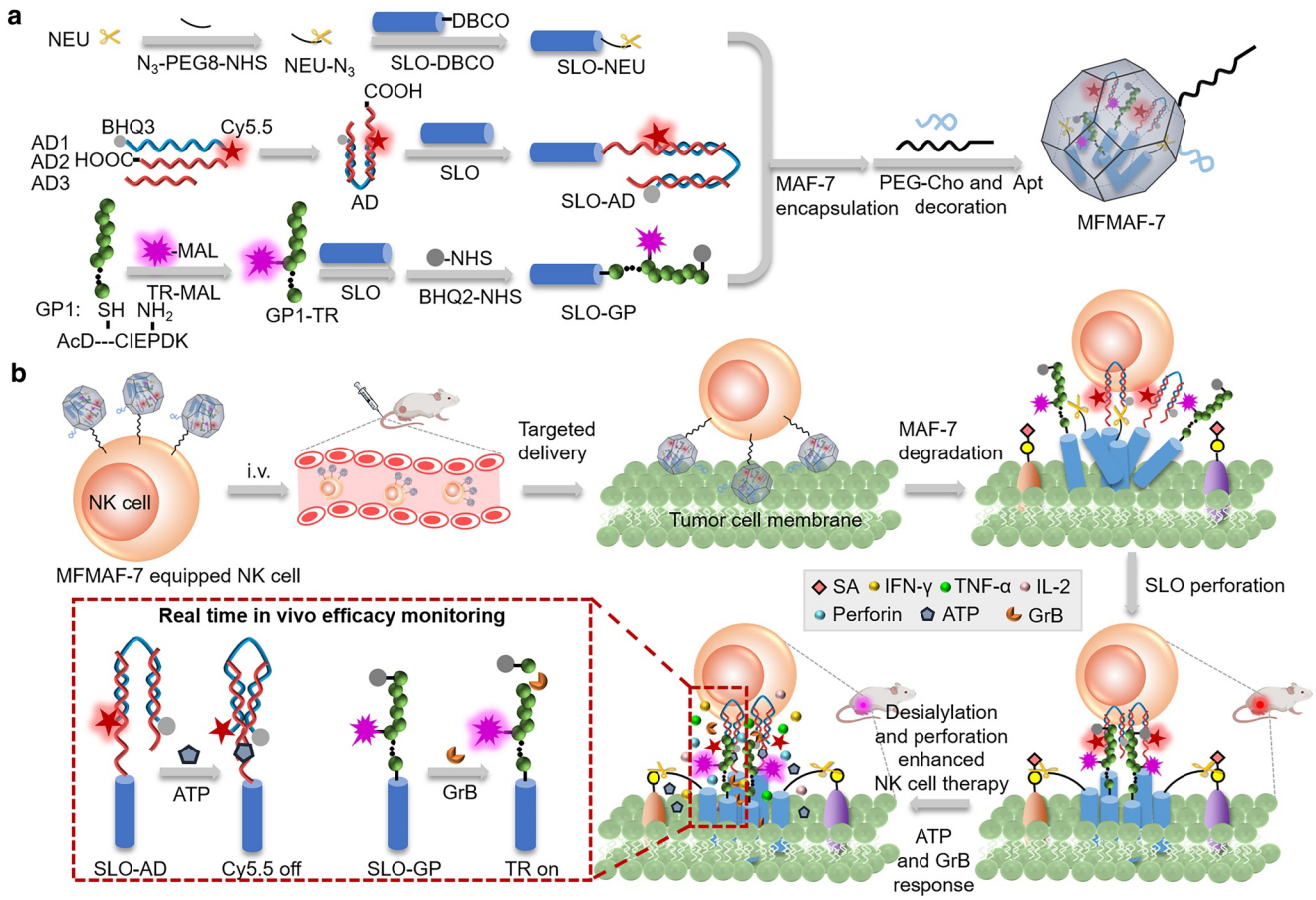

FIGURE 1 Schematic illustration of desialylation and perforation enhanced cancer immunotherapy with real time efficacy monitoring. (a) Preparation of SLO-NEU, SLO-AD, SLO-GP and MFMAF-7. (b) Cancer immunotherapy and efficacy monitoring mechanism with MFMAF-7 engineered NK cells. After i.v. injection and targeted delivery into tumor region, MFMAF-7 on NK cells is degraded to release SLO-NEU, SLO-AD and SLO-GP, which perforate on tumor cells and cleave sialic acids to enhance the NK cell therapy and response the levels of ATP and GrB for real time assessment of the efficacy.

assay. SLO-AD exhibited strong Cy5.5 fluorescence at 704 nm, which obviously decreased after incubation with ATP (Figure 2a), demonstrating its sensitive response to ATP. In contrast, SLO-GP did not exhibit the fluorescence of TR at 610 nm (Figure 2b), indicating the complete quenching of TR fluorescence by BHQ2. After incubating SLO-GP with GrB, the TR fluorescence was observed, demonstrating its strong response to GrB. Moreover, the fluorescent intensity (FI) of SLO-AD or SLO-GP responded to the change of ATP or GrB concentration (Figure S1c,d), which demonstrated the feasibility of using SLO-AD and SLO-GP to detect the concentrations of ATP and GrB.

The functions of SLO-AD and SLO-GP on tumor cell membranes were further demonstrated by confocal laser scanning microscope (CLSM) imaging of cells. After treated with SLO-AD or SLO-GP, 4T1 cells were incubated with different concentrations of ATP or GrB, which resulted in attenuated Cy5.5 fluorescence or enhanced TR fluorescence along with the increasing concentration (Figure 2c,d and Figure S2). With the increasing incubation time, the similar changes were observed at the same ATP or GrB concentration (Figure S3). These results demonstrated the efficient response of SLO-AD and SLO-GP to ATP and GrB on the cell membrane.

To investigate the SA-cleaving function of SLO-NEU on the cell membrane, 4T1 cells were treated with SLO-NEU or NEU and then incubated with Cy3-labeled Sambucus Nigra lectin (Cy3-SNA) to specifically recognize SA[34] on the cell membrane. Both the SLO-NEU and NEU treated cells exhibited negligible Cy3 fluorescence compared to the untreated cells (Figure S4a), which demonstrated the similar SA-cleaving function of SLO-NEU to the native NEU on cell membrane. The perforating function of the SLO conjugates was investigated by incubating the SLO and SLO conjugates pre-treated 4T1 cells with propidium iodide (PI). Obvious PI fluorescence was observed in all the SLO, SLO-AD, SLO-GP and SLO-

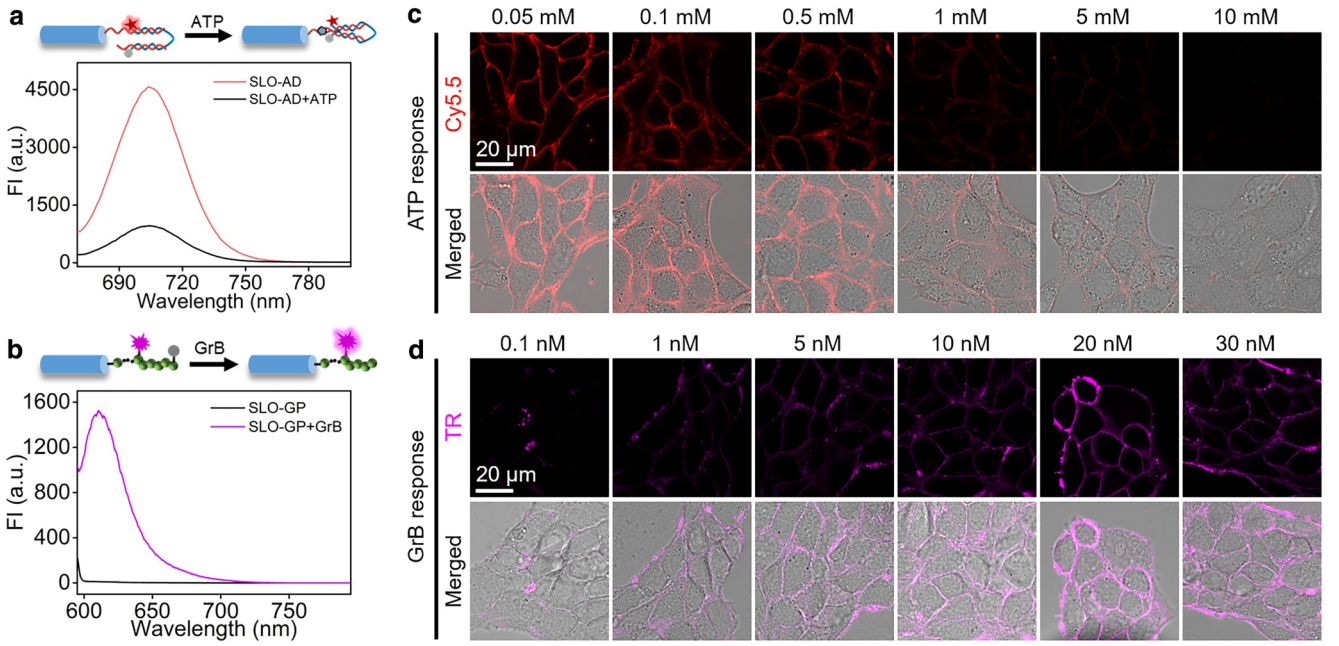

FIGURE 2 Responses of SLO-AD and SLO-GP to ATP and GrB. (a, b) Schematic illustration and the variation of fluorescence spectra of SLO-AD (a) or SLO-GP (b) after treatment with ATP or GrB in vitro. (c, d) CLSM images of 4T1 cells after incubation with SLO-AD (c) or SLO-GP (d) and then treated with different concentrations of ATP (c) or GrB (d) at 37°C for 1 h. Scale bars: 20 μm.

NEU pre-treated cells, opposite to untreated cells (Figure S4b), demonstrating the perforating function of these SLO conjugates on the tumor cell membrane.

The interactions between SLO conjugates and NK cells were also investigated by incubating the mixture of SLO conjugates with NK cells, which did not show Cy5.5 fluorescence on NK cells (Figure S5a). After the SLO and SLO conjugates pre-treated NK cells were further incubated with PI, these cells did not also exhibit any PI fluorescence (Figure S6a), indicating that SLO and SLO conjugates could not perforate on NK cells. These phenomena were agreed with the previous report of the perforation preference of the perforins during the immune-killing process,[35] which helped to preserve NK cell viability during the therapy.

2.2 | SLO conjugates enhanced in vitro immune-killing

The NK cell immune-killing enhanced by SLO conjugates was in vitro investigated by CCK8 assay of the 4T1 cells treated with different combinations of SLO conjugates and NK cells at the NK/4T1 ratio of 10:1 (Figure 3a). In the absence of NK cells, the 4T1 cells treated with the mixture of SLO-AD, SLO-GP and SLO-NEU (Group 2) exhibited 44% decrease of tumor cell viability (Figure 3b), which indicated the efficient perforation of the SLO conjugates. In contrast, the 4T1 cells treated with individual NK cells (Group 3) or NK cells together with AD and GP (Group 4) only exhibited 22% decrease of tumor cell viability (Figure 3b), indicating the limited immune-killing efficiency of individual NK cells and the negligible effect of AD and GP probes. However, the 4T1 cells treated with NK cells cooperated with NEU (Group 5), SLO-NEU (Group 6), the mixture of SLO-AD, SLO-GP and SLO (Group 7), and the mixture of SLO-AD, SLO-GP and SLO-NEU (Group 8) exhibited gradually increasing enhancement of immune-killing, while Group 8 exhibited the highest immune-killing efficiency with 64% decrease in tumor cell viability (Figure 3b). These results demonstrated the efficient enhancement of the immune-killing by SLO conjugates, which could be attributed to the desialylation by NEU and the perforation by all the SLO conjugates.

To further verify the enhancement of the immune-killing, the cytokines secreted from NK cells during the in vitro immune-killing were analyzed by ELISA. Groups 4–8 showed the gradually increased levels of all cytokines such as IFN-γ (Figure 3c), TNF-α (Figure 3d), IL-2 (Figure 3e), perforin (Figure 3f) and GrB (Figure 3g), which was in good agreement with the decreases of cell viability (Figure 3b). Thus, the desialylation by NEU and perforation by SLO conjugates could exactly enhance the

a

Group	Treatment of 4T1 cells			NK
(1)	-	-	-	-
(2)	SLO-AD	SLO-GP	SLO-NEU	-
(3)	-	-	-	+
(4)	AD	GP	-	+
(5)	-	-	NEU	+
(6)	-	-	SLO-NEU	+
(7)	SLO-AD	SLO-GP	SLO	+
(8)	SLO-AD	SLO-GP	SLO-NEU	+
(9)	MFMAF-7			+
(10)	Degraded MFMAF-7			+

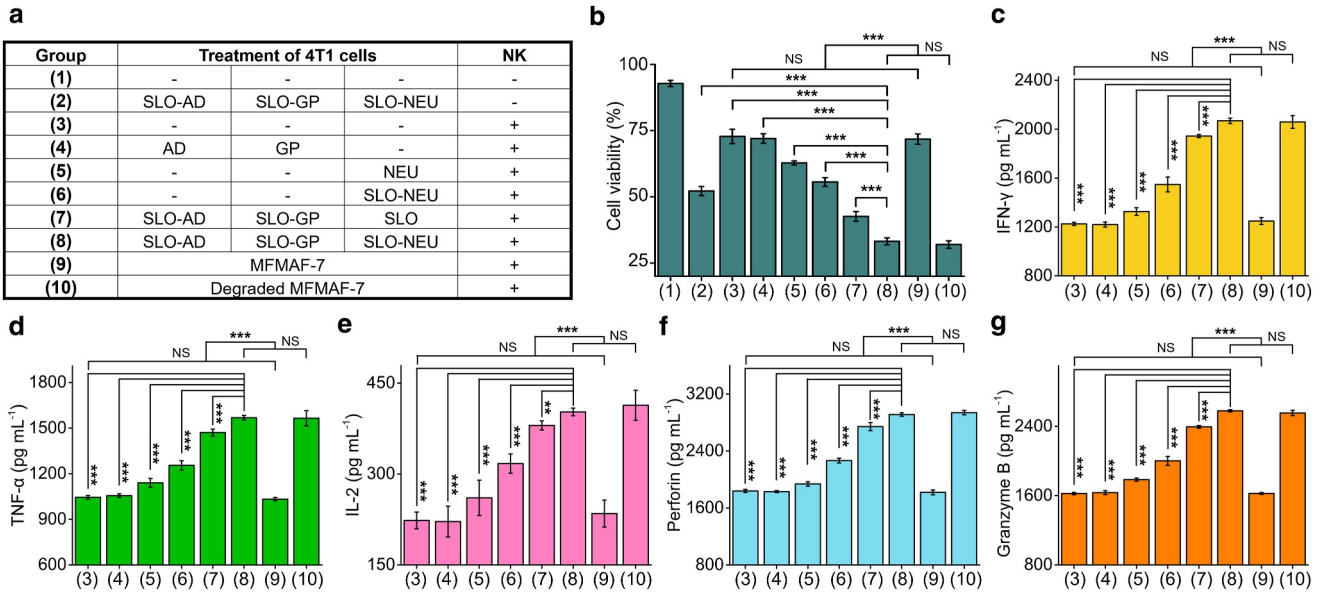

FIGURE 3 SLO conjugates enhanced in vitro immune-killing. (a) Group list of 4T1 cells with different treatments. (b) Cell viability of 4T1 cells from groups (1)–(10). (c-g) ELISA analysis of secreted cytokines from groups (3)–(10). Statistical analysis was performed by unpaired two-tailed *t*-tests (***$p < 0.001$; **$p < 0.01$; NS, not significant), $n = 5$.

in vitro immune-killing of tumor cells, and their integration could efficiently maximize the enhancement.

2.3 | Characterization and performance of MFMAF-7

The MAF-7 was prepared following the previous report,[36] and displayed a uniform rhombic dodecahedral structure with a diameter of about 137 nm (Figure S7a). As the proteins encapsulated in hydrophilic MAF-7 could retain protein activity[37] even exposed in plasma, the mixture of SLO-AD, SLO-GP and SLO-NEU was encapsulated in MAF-7 by one-pot synthesis to form SLO-AD/GP/NEU@MAF-7, which was further coated with dopamine polyethylene glycol 3350 cholesterol (PEG-Cho) and then modified with tumor-targeting Apt via non-covalent modification to obtain MFMAF-7. The encapsulation efficiency of SLO conjugates was determined to be 72.3 ± 6.5% by bicinchoninic acid (BCA) protein assay kit (Figure S8a). The MFMAF-7 displayed a similar morphology with a diameter of about 115 nm (Figure S7b). The smaller diameter of MFMAF-7 resulted from the presence of proteins during its synthesis.[36] The successful modification of PEG was characterized by MALDI-TOF mass spectrometry. Compared to the SLO-AD/GP/NEU@MAF-7, the MFMAF-7 exhibited a characteristic spectrum with an equally spaced 44 m/z value of PEG (Figure S7c). After coating PEG, SLO-AD/GP/NEU@MAF-7@PEG showed declined positive zeta potential due to the chelation between the phenolic group of dopamine-PEG and external Zn^{2+} sites on the MAF-7,[38] while MFMAF-7 showed negatively-charged surface (Figure S7d), indicating the presence of Apt on MFMAF-7. The drug release of MFMAF-7 was also determined by the BCA protein assay kit (Figure S8b), which exhibited a strong pH dependence. At pH 6.5, over 50% of the encapsulated drug was released within the first 2 h, followed by a sustained and slower release phase, ultimately reaching a cumulative release of 81.6% at 50 h. In contrast, only 10.5% of the drug was released at pH 7.4 after 50 h, which demonstrated that MFMAF-7 remained stable in the physiological environment but can rapidly release the encapsulated drug in the acidic tumor microenvironment.

The performance of MFMAF-7 was first investigated in vitro by fluorescence spectrometry. Similar to the mixture of SLO-AD, SLO-GP and SLO-NEU, MFMAF-7 exhibited obvious fluorescence of Cy5.5, while the PEG and Apt modified MAF-7 (MAF-7@PEG/Apt) did not exhibit any fluorescence (Figure S9a), demonstrating the encapsulation of SLO conjugates. After degrading the MFMAF-7 in an acidic solution (pH 6.5) and then treated with ATP or GrB, the mixture exhibited an obvious decrease of Cy5.5 fluorescence or the appearance of TR fluorescence (Figure S9b). Thus, the SLO-AD and SLO-GP released from the degraded MFMAF-7 could maintain their functions responding to ATP and GrB, respectively.

After 4T1 cells were respectively treated with the mixture of SLO-AD, SLO-GP and SLO-NEU, SLO-AD/GP/NEU@MAF-7, and the degraded SLO-AD/GP/

NEU@MAF-7, they were further stained with PI or Cy3-SNA to verify the perforating or SA-cleaving functions. As a result, obvious PI fluorescence was observed on the SLO-AD/GP/NEU and the degraded SLO-AD/GP/NEU@MAF-7 treated cells, but the SLO-AD/GP/NEU@MAF-7 treated cells did not show any change (Figure S10). Meanwhile, the Cy3 fluorescence appeared on the control and SLO-AD/GP/NEU@MAF-7 cells and disappeared from the SLO-AD/GP/NEU and degraded SLO-AD/GP/NEU@MAF-7 treated cells (Figure S10). These phenomena indicated that the degradation of SLO-AD/GP/NEU@MAF-7 could completely recover the perforating and SA-cleaving functions of the SLO conjugates.

The ATP and GrB responding functions of MFMAF-7 were further verified by incubating the SLO-AD/GP/NEU@MAF-7 and the degraded SLO-AD/GP/NEU@-MAF-7 treated 4T1 cells with ATP and GrB, respectively (Figure 4a). As expected, the CLSM images of the degraded SLO-AD/GP/NEU@MAF-7 treated 4T1 cells exhibited obvious Cy5.5 fluorescence, which greatly decreased or even disappeared after incubation with ATP (Figure 4a). In contrast, tiny TR fluorescence was observed on the degraded SLO-AD/GP/NEU@MAF-7 treated 4T1 cells and became stronger upon GrB incubation (Figure 4a). These phenomena indicated that the SLO-AD and SLO-GP released from the degraded SLO-AD/GP/NEU@MAF-7 could maintain the ATP and GrB responding functions. To verify the simultaneous responses of the degraded MFMAF-7 to ATP and GrB (Figure 4b), the fluorescence resonance energy transfer (FRET) between TR and Cy5.5 in SLO-AD and SLO-GP was first excluded. As shown in Figure S11, the 4T1 cells treated with the mixture of SLO-AD, SLO-GP1-TR and SLO-NEU showed both TR and Cy5.5 fluorescence under their excitation wavelength, while only TR fluorescence was observed under TR excitation, indicating the absence of FRET between TR and Cy5.5. Therefore, the simultaneous responses of the released SLO-AD and SLO-GP from degraded MFMAF-7 (Figure 4c) could be attributed to the presence of ATP and GrB. Moreover, the responses (fluorescence decrease and increase) become greater with increasing incubation time of ATP and GrB (Figure S12), providing a real time monitoring method of the in vivo NK cell therapy efficacy through in situ visualizing the levels of ATP released from the dying tumor cells and GrB released from NK cells.

The direct cytotoxicity of MFMAF-7 was evaluated by CCK-8 assay of 4T1 cells treated with different concentrations of MFMAF-7 under different pH conditions (Figure S13a). The 4T1 cells treated with 0–200 μg/mL of MFMAF-7 under pH 7.4 maintained high cell viability, which demonstrated the material safety of MFMAF-7. In contrast, the 4T1 cells treated with 0–100 μg/mL of MFMAF-7 under pH 6.5 exhibited significant and dose-dependent decrease of the cell viability, which demonstrated the therapeutic performance of the released drugs. Thus, 100 μg/mL was selected as the optimal dose of MFMAF-7 for subsequent cellular experiments.

2.4 | Engineering of NK cells with MFMAF-7

After incubating NK cells with MFMAF-7, the engineered NK cells exhibited obvious Cy5.5 fluorescence of MFMAF-7 on the cell surface (Figure S5b). To investigate the location of MFMAF-7 on NK cells, 3,3′-Dioctadecyloxacarbocyanine perchlorate (Dio) was used to stain the NK cell membrane. After incubating the Dio-stained NK cells with MFMAF-7 at 37°C for 10 min, a co-localized Dio and Cy5.5 fluorescence signal was observed (Figure S5c), which indicated that MFMAF-7 was attached onto the NK cell surface. The NK cells incubated with the degraded MFMAF-7 or then stained with PI did not show Cy5.5 or PI fluorescence (Figure S5d and S6b), which was similar to the NK cells incubated with the mixture of SLO-AD, SLO-GP and SLO-NEU (Figure S5a and S6a). Thus, the SLO conjugates released from the degraded MFMAF-7 maintained the same perforation preference against NK cells, which was beneficial for NK cell therapy.

The effector-to-target (E: T) ratio of the immune-killing between MFMAF-7 engineered NK cells and 4T1 cells was optimized by CCK-8 assay (Figure S13b). The cytotoxic response reached a plateau at an E:T ratio of 10:1, indicating maximal immune-killing efficacy. The E: T ratio of 10:1 was then selected for subsequent immune-killing experiments.

The performance of MFMAF-7 engineered NK cells in the in vitro immune-killing of tumor cells was investigated by CCK8 (Figure 3b) and ELISA (Figure 3c–g). After 4T1 cells were treated with MFMAF-7 engineered NK cells (Group 9), they did not exhibit significant differences in cell viability (Figure 3b) and cytokine secretion (Figure 3c–g) compared to these treated with individual NK cells (Group 3), which indicated the efficient inhibition of the SLO conjugations by MAF-7 encapsulation. Meanwhile, the 4T1 cells treated with the degraded MFMAF-7 engineered NK cells (Group 10) exhibited similar enhancement of the immune-killing (Figure 3b) and cytokine secretion (Figure 3c–g) to these incubated with SLO-AD/GP/NEU treated NK cells (Group 8), which further demonstrated the functions of SLO conjugations released from the degraded MFMAF-7 to enhance the immune-killing of tumor cells.

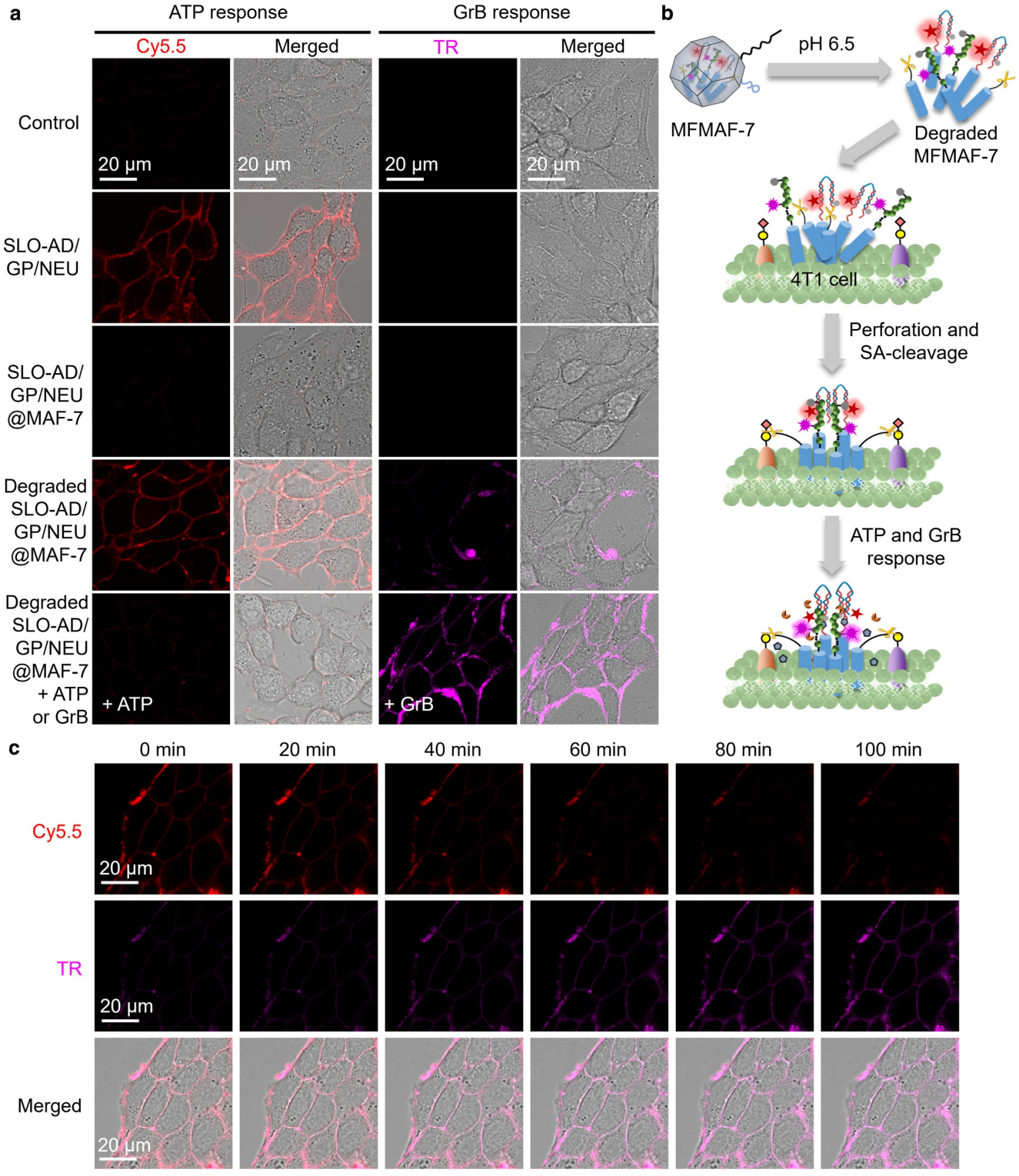

FIGURE 4 ATP and GrB responses of degraded MFMAF-7 on 4T1 cells. (a) CLSM images of 4T1 cells after incubation with PBS (Control), SLO-AD/GP/NEU, SLO-AD/GP/NEU@MAF-7, degraded SLO-AD/GP/NEU@MAF-7 and the mixture of degraded SLO-AD/GP/NEU@MAF-7 with ATP or GrB. (b) Schematic illustration of simultaneous ATP and GrB responses of degraded MFMAF-7 on 4T1 cells. (c) Continuous CLSM images of 4T1 cells incubated with degraded MFMAF-7 and then the mixture of 5 mM ATP and 20 nM GrB at 37°C for different times.

To investigate the responsiveness of the MFMAF-7 at the cellular level, the MFMAF-7 engineered NK cells were co-cultured with 4T1 cells for different times and monitored by CLSM imaging (Figure S14). At the initial stage (0 h), the engineered NK cells displayed strong Cy5.5 fluorescence from the loaded MFMAF-7 and negligible TR fluorescence. After co-cultured with 4T1 cells for different times, the TR fluorescence gradually emerged and intensified, while the Cy5.5 fluorescence progressively diminished, which was consistent with the phenomena of cells exogenously adding ATP or GrB (Figures 2 and 4), indicating the successful release of GrB and ATP from activated NK cells and dying 4T1 cells and the visual capability of the designed strategy.

2.5 | In vivo NK cell therapy and real time efficacy monitoring with MFMAF-7 engineered NK cells

To verify the desialylation and perforation enhanced NK cell therapy and real time efficacy monitoring with MFMAF-7 engineered NK cells, 4T1 tumor xenograft mouse models with a tumor volume of ~80 mm^3 were established, and randomly divided into eight groups to respectively receive intravenous injections of (1) saline, (2) NK cells, (3) AD/GP/NEU@MAF-7@PEG/Apt equipped NK cells, (4) SLO-AD/GP/NEU@MAF-7@PEG equipped NK cells, (5) MFMAF-7, (6) SLO-NEU@MAF-7@PEG/Apt equipped NK cells, (7) SLO-AD/GP@MAF-7@PEG/Apt equipped NK cells and (8) MFMAF-7 engineered NK cells every other day for 14 days, respectively (Figure 5a). In the 14 days of treatments, neither discernible difference of body weight (Figure S15a) nor abnormal pathological change of the heart, liver, spleen, lung and kidney (Figure S16) nor any significant abnormal accumulation or excessive infiltration of F4/80-positive macrophages in immunohistochemical staining of liver and spleen (Figure S17) were observed in all groups of mice. The drug distribution 12 h post-injection revealed distinct patterns across different treatment groups (Figure S18), while Group 8 exhibited the most efficient tumor-targeting with highest tumor uptake and lowest off-target accumulation, which indicated the negligible side effects of the designed strategy.

To monitor the efficacy in real time, the mice were subjected to in vivo imaging within 48 h after the first injection (Figure 5c and Figure S19). The weak Cy5.5 fluorescence from the blocked SLO-AD could be conveniently used as the tracking signal of the SLO conjugates before reaching the tumor region. In the absence of SLO, the probes could not retain in tumor region, thus did not show any fluorescence within 48 h (Group 3), which led to tumor volumes similar to those of Group 2 after intravenous injection for 48 h (Figure 5b), indicating very low therapy efficacy and the importance of SLO mediated perforation to enhance the NK cell therapy. Different from Group 3, Group 4 exhibited obvious Cy5.5 fluorescence at 8 h after injection due to the presence of SLO conjugates released from MAF-7, while Groups 5, 7 and 8 showed earlier Cy5.5 fluorescence than Group 4. Moreover, their fluorescence intensity was also stronger at the same time, indicating the faster Apt-mediated target delivery to the tumor region,[24] and the higher tumor therapy efficacy, which led to smaller tumor volume (Figure 5b). Groups 5, 7 and 8 showed the strongest Cy5.5 fluorescence at 21, 12 and 12 h after injections, which then gradually decreased over time. The intratumoral ATP levels of Groups 1, 7 and 8 were measured by the ATP Chemiluminescence Assay Kit (Figure S20). The intratumoral ATP level of Group 8 was the highest compared to those of Groups 1 and 7, which demonstrated that the MFMAF-7 engineered NK cells can most effectively induce the immunogenic tumor cell death to release the most massive ATP. In contrast, the TR fluorescence appeared in Groups 5, 7 and 8, and gradually increased from 8 to 48 h after injections due to the release of GrB from the NK cells. These phenomena indicated that the SLO conjugates successfully responded to the increased expression of ATP and GrB during the immune-killing process. Among these groups, Group 8 exhibited the most drastic decrease in Cy5.5 fluorescence after 12 h and dropped to the lowest levels by 48 h, indicating the most massive and efficient death of tumor cells (Figure 5c and Figure S19a). Meanwhile, Group 8 displayed a significantly faster response in TR fluorescence at 21 h compared to other groups, which indicated the earlier immune synapse formation and faster GrB release, leading to the rapid onset of immune-killing (Figure 5c and Figure S19b). Besides, Group 8 exhibited the consistently lowest tumor growth throughout the treatment course (Figure S15b) and the longest survival time (Figure S15c), indicating the highest tumor therapy efficacy. The hematoxylin and eosin (H&E) and terminal deoxynucleotidyl transferase dUTP Nick end labeling (TUNEL) staining tissue slices of the tumors dissected from Group 8 showed the largest necrotic area in comparison to these from Groups 1–7 (Figure 5d), further demonstrating the strongest NK cell therapy efficacy of cancer with MFMAF-7 engineered NK cells. Thus, the designed strategy could exactly achieve the in vivo monitoring of NK cell therapy efficacy in real time.

The effect of desialylation in the tumor region on NK cell therapy was also investigated by staining the sectioned tumor tissues with Cy3-labeled Sambucus Nigra Lectin (Cy3-SNA) and DAPI (Figure S21). After the

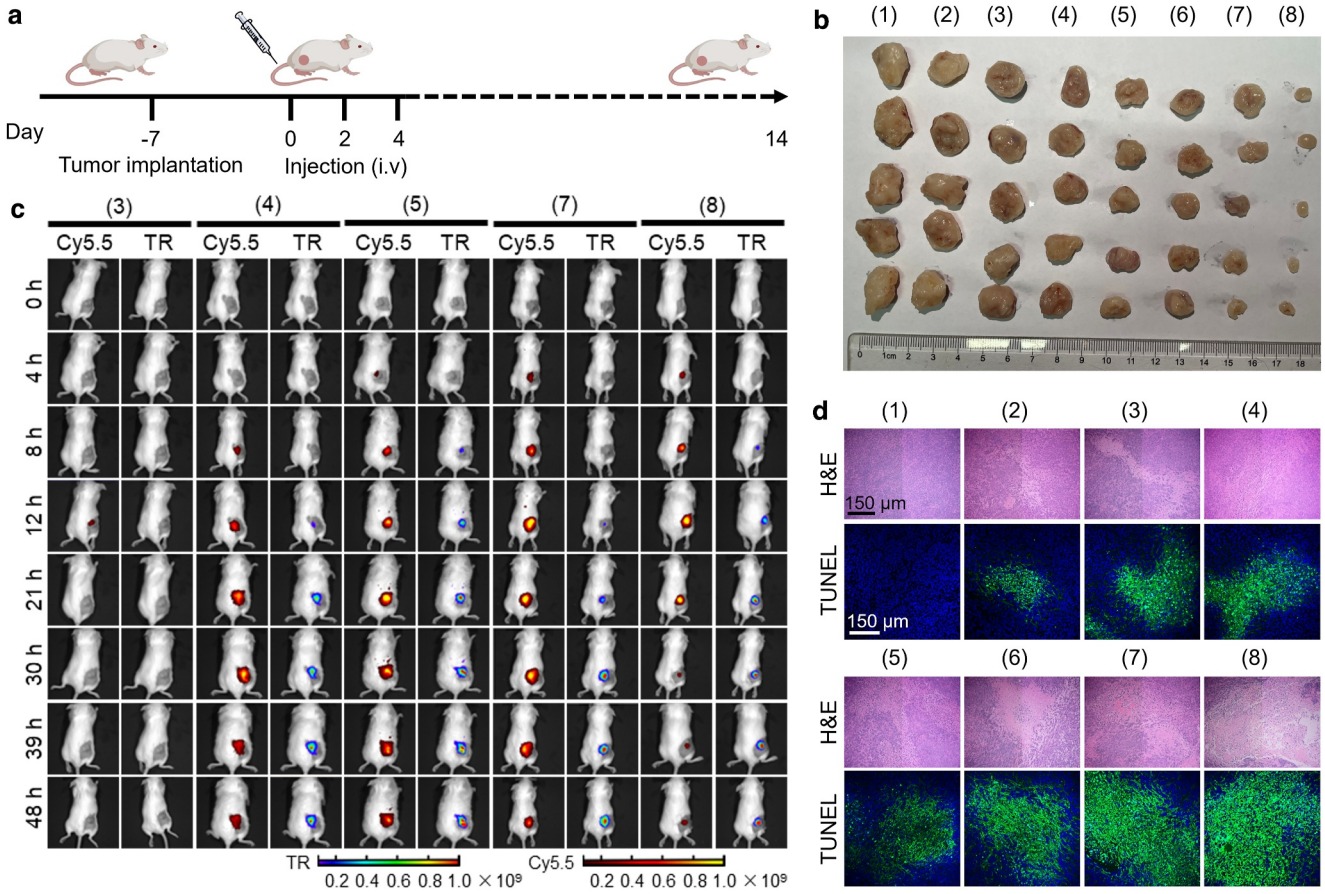

FIGURE 5 In vivo NK cell therapy and real time efficacy monitoring of tumor-bearing mice. (a) Schematic illustration of the implantation and treatment on 4T1 tumor-bearing mice. (b) Photo of tumors dissected from different groups of 4T1 tumor-bearing mice. Groups (1): saline, (2): NK cells, (3): AD/GP/NEU@MAF-7@PEG/Apt equipped NK cells, (4): SLO-AD/GP/NEU@MAF-7@PEG equipped NK cells, (5): MFMAF-7, (6): SLO-NEU@MAF-7@PEG/Apt equipped NK cells, (7): SLO-AD/GP@MAF-7@PEG/Apt equipped NK cells, and (8): MFMAF-7 engineered NK cells. (c) Continuous in vivo fluorescence imaging of 4T1 tumor-bearing mice after the first injection. (d) Histology and CLSM images of tumor sections from different groups of 4T1 tumor-bearing mice after H&E and TUNEL staining.

tumor sections from different groups of 4T1 tumor-bearing mice were stained with Cy3-SNA and DAPI, Groups 5, 6 and 8 exhibited significant decrease of the Cy3 fluorescence compared to the other groups, which indicated the efficient SA-cleavage of the SLO-NEU on cell membrane. As for Groups 3 and 4, the SA level in the tumor region was similar to those of Groups 1, 2 and 7 in the absence of NEU, indicating the importance of both anchoring NEU on cell surface and the Apt targeted delivery for efficient cleavage of SA. Therefore, it could be concluded that the improved NK cell therapy efficacy could be attributed to both the desialylation and the perforation of extrinsic MFMAF-7 engineered NK cells.

Compared to the existing clinical NK therapies, this strategy exhibits advantages for the treatment of tumors with dense extracellular matrix and hypersialylation, which can also provide real time efficacy monitoring rather than the delayed assessments by tumor volume variation or physiological analysis. As for the potential clinical applications, this strategy may be limited by the standardization, cost and complexity of the nanomedicine preparation.

3 | CONCLUSIONS

This work designs a powerful nanomedicine MFMAF-7 to engineer extrinsic NK cells for enhancing the targeted NK cell therapy and real time monitoring of in vivo therapy efficacy. The greatly enhanced therapy efficacy and monitoring capacity have been achieved by encapsulating SLO-NEU/AD/GP in the nanomedicine and targeted delivery of the engineered NK cells to tumor region, which results in the degradation of MFMAF-7 to release encapsulated SLO-NEU/AD/GP for obtaining their perforating function on tumor cells, the desialylation of SLO-NEU and the fluorescence responses of SLO-AD/GP to the level changes of ATP and GrB during the

NK cells-mediated immune-killing, respectively. The engineering and targeted delivery of NK cells can be performed via coating PEG-Cho and modifying Apt on SLO-AD/GP/NEU@MAF-7. The feasibility and practical application of the MFMAF-7 engineered NK cells in efficiently enhanced NK cell therapy and monitoring the in vivo NK cell therapy efficacy in real time have been demonstrated with 4T1 tumor xenograft mouse models. By simple replacement of the functional and responsive components, this strategy can be easily expanded to regulate and monitor other disease related biomolecules, which provides a potential platform for the development of novel therapeutic and efficacy monitoring methods.

4 | EXPERIMENTAL SECTION

Preparation of SLO-AD, SLO-GP, SLO-NEU and MFMAF-7: AD was prepared following a previous method[31] by heating the mixture of AD1, AD2 and AD3 (100 μM in PBS) at 95°C for 5 min and then cooling naturally. To prepare SLO-AD, AD (100 μM) was first mixed with EDC (10 mM) and NHS (25 mM) in MES buffer (0.1 M MES, 0.5 M NaCl, pH 6.0) at room temperature for 15 min. After regulating the pH to 7.0, the mixture was added with SLO (10 μM) to incubate at room temperature for 2 h. The mixture was then filtered with 100 kDa MWCO membrane to purify the obtained SLO-AD.

SLO-GP was prepared by reacting GP1 (100 μM) with TR-MAL (300 μM) in DMF at room temperature overnight, and then regulating the pH to 7.0 and adding SLO (10 μM) to incubate at room temperature for 2 h. The mixture was filtered with 30 kDa MWCO membrane to purify SLO-GP1-TR. After BHQ2-NHS (100 μM) was added to the obtained SLO-GP1-TR to incubate at room temperature for 2 h, the mixture was filtrated with 30 kDa MWCO membrane to purify the obtained SLO-GP1-TR/BHQ2 (SLO-GP).

SLO-NEU was prepared by mixing SLO-DBCO and NEU-N_3 following our previous method.[17] SLO-DBCO was first prepared by mixing SLO (0.55 mM) and DBCO-sulfo-NHS ester (47 mM) at room temperature for 2 h, and then filtrating the mixture with 30 kDa MWCO membrane. Similarly, NEU-N_3 was prepared by mixing NEU (0.02 mM) and N_3-PEG8-NHS (0.1 mM) at room temperature for 2 h, which was then mixed with SLO-DBCO (0.1 mM) at room temperature for 2 h and filtrated with 100 kDa MWCO membrane to obtain SLO-NEU.

The MFMAF-7 was prepared following a previous method.[36] Briefly, $Zn(NO_3)_2{\cdot}6H_2O$ (50 mM), Hmtz (250 mM), SLO-AD (100 U mL^{-1}), SLO-GP (100 U mL^{-1}) and SLO-NEU (100 U mL^{-1}) were mixed and aged at room temperature for 24 h. The resulting precipitates were centrifuged at 10,000 rpm for 10 min and washed three times to form SLO-AD/GP/NEU@MAF-7.

Then, 1 mg of SLO-AD/GP/NEU@MAF-7 was incubated with 3 mg of PEG-Cho and then 10 μM of Apt in 1 mL Tris-HCl buffer (pH 7.4, 10 mM) at 37°C for 6 h to obtain MFMAF-7. The controls including AD/GP/NEU@MAF-7@PEG/Apt, SLO-AD/GP/NEU@MAF-7, SLO-AD/GP/NEU@MAF-7@PEG, SLO-NEU@MAF-7@PEG/Apt and SLO-AD/GP@MAF-7@PEG/Apt were prepared with the same procedure.

Drug loading efficiency: After the synthesis of SLO-AD/GP/NEU@MAF-7, the mixture was centrifuged at 12,000 rpm for 15 min to separate the precipitate and supernatant. The supernatant was collected and lyophilized, and its protein concentration was determined using a BCA protein assay kit according to a standard curve. Drug Loading Content (%) = (Mass of Loaded Drug/Total Mass of Drug-Loaded System) × 100% and Encapsulation Efficiency (%) = (Mass of Loaded Drug/Total Mass of Initial Input Drug) × 100%.

Release Kinetics of MFMAF-7: MFMAF-7 (1 mg) was dispersed in 1 mL of PBS buffer (pH 6.5, simulating the tumor microenvironment) and incubated at 37°C. At predetermined time points (0, 1, 2, 4, 8, 12, 24, 48 h), the samples were centrifuged at 10,000 rpm for 10 min. The supernatant was collected and lyophilized. The concentration of the released protein was then determined using the BCA assay.

Stability: MFMAF-7 (1 mg) was dispersed in 1 mL of PBS buffer (pH 7.4, simulating the normal physiological environment) and incubated at 37°C. At designated time intervals (0, 1, 2, 4, 8, 12, 24, 48 h), the samples were centrifuged at 10,000 rpm for 10 min. The supernatant was collected and lyophilized, followed by the quantification of the released protein concentration using the BCA assay.

CLSM imaging of treated tumor cells: 4T1 cells were seeded on confocal dishes overnight and washed three times with HBSS. To investigate the perforating and SA-cleaving functions of SLO conjugates, the cells were respectively incubated with 300 U mL^{-1} of SLO, SLO-AD, SLO-GP, SLO-NEU, the mixture of SLO-AD, SLO-GP and SLO-NEU (100 U mL^{-1} for each), 0.1 μM NEU, MFMAF-7, and the degraded MFMAF-7 at 37°C for 20 min, and then stained with PI or Cy3-SNA (10 μg mL^{-1}) at 4°C for 60 min before subjecting to CLSM imaging.

To investigate the ATP and GrB responses of SLO conjugates, 4T1 cells seeded on dishes were incubated with 300 U mL-1 of SLO-AD or SLO-GP at 37°C for 20 min, and then with different concentrations of ATP or GrB at 37°C for different times. The simultaneous responses of degraded MFMAF-7 to ATP and GrB were

verified by incubating degraded MFMAF-7 with 4T1 cells at 37°C for 20 min, and then the mixture of 5 mM ATP and 20 nM GrB at 37°C for different times.

To investigate the responsiveness of the MFMAF-7 construct at the cellular level, the 4T1 cells were co-cultured with MFMAF-7 engineered NK cells (E: T = 10:1) and monitored after 0 h, 4 h, 8 h and 12 h under pH 6.5 at 37°C.

When performing the CLSM imaging, the PI channel was collected from the emission signal between 555 and 625 nm under a 535 nm excitation. The Cy3 channel was collected from the emission signal between 555 and 640 nm under a 543 nm excitation. The Cy5.5 channel was collected from the emission signal between 670 and 795 nm under a 650 nm excitation. The TR channel was collected from the emission signal between 600 and 645 nm under a 589 nm excitation.

Engineering of NK cells and CLSM imaging: The engineering of NK cells was performed by incubating NK cells with MFMAF-7 at 37°C for 10 min, and then washing them with PBS for three times. To verify the location of MFMAF-7 on NK cells, they were stained with Dio and then incubated with MFMAF-7 at 37°C for 10 min. Meanwhile, NK cells were incubated with 300 U mL^{-1} of SLO, the mixture of SLO-AD, SLO-GP and SLO-NEU (100 U mL^{-1} for each) or the degraded MFMAF-7 at 37°C for 20 min, and then washed three times with HBSS and stained with PI (10 μg mL^{-1}) at 4°C for 60 min. The obtained NK cells were immobilized on a poly-L-lysine treated confocal dish for 10 min to perform CLSM imaging. The Dio channel was collected from the emission signal between 505 and 555 nm under a 488 nm excitation.

Assay of the viability of tumor cells and the cytokines secreted from NK cells: 4T1 cells seeded on dishes were respectively incubated with 0, 10, 25, 50, 100, 200 μg/mL of MFMAF-7 under pH 6.5 or 7.4 at 37°C for 4 h, or MFMAF-7 engineered NK cells with the E: T = 1:1, 2.5:1, 5:1, 10:1, 20:1 under pH 6.5 at 37°C for 4 h, or (1) PBS, (2) the mixture of SLO-AD, SLO-GP and SLO-NEU (100 U mL^{-1} for each), (3) PBS, (4) the mixture of AD and GP (0.1 μM for each), (5) 0.1 μM NEU, (6) 100 U mL^{-1} of SLO-NEU, (7) the mixture of SLO-AD, SLO-GP and SLO (100 U mL^{-1} for each), (8) the mixture of SLO-AD, SLO-GP and SLO-NEU (100 U mL^{-1} for each), (9) MFMAF-7, and (10) degraded MFMAF-7 at 37°C for 1 h. The groups (3)-(10) were further incubated with NK cells (with a NK: 4T1 ratio of 10:1) at 37°C for 4 h before subjecting to the CCK8 assay. The supernatants of groups (3)–(10) containing secreted IFN-γ, TNF-α, IL-2, perforin and GrB were collected by centrifugation for ELISA quantification of cytokines.

Animal experiments: Pathogen-free female BALB/c mice (5 weeks old) were obtained from GemPharmatech Co. Ltd. (China). To prepare the 4T1 tumor xenograft mouse model, 2×10^6 of 4T1 cells suspended in PBS were subcutaneously inoculated into the hind leg of each mouse. After tumor volume reached about 80 mm^3, the 4T1 tumor-bearing BALB/c mice were randomly divided into 8 groups ($n = 5$). These groups were intravenously injected in tail every other day for 14 days with 100 μL of (1) saline, (2) NK cells (10^7 cells containing 2000 unit/mL of IL-2 to promote the survival and expansion of NK cells in vivo NK-mediated immune-killing[23, 39]), (3) AD/GP/NEU@MAF-7@PEG/Apt equipped NK cells (10^7 cells containing 2000 unit/mL of IL-2), (4) SLO-AD/GP/NEU@MAF-7@PEG equipped NK cells (10^7 cells containing 2000 unit/mL of IL-2), (5) MFMAF-7, (6) SLO-NEU@MAF-7@PEG/Apt equipped NK cells (10^7 cells containing 2000 unit/mL of IL-2), (7) SLO-AD/GP@MAF-7@PEG/Apt equipped NK cells (10^7 cells containing 2000 unit/mL of IL-2), and (8) MFMAF-7 engineered NK cells (10^7 cells containing 2000 unit/mL of IL-2), respectively.

The in vivo mice imaging was performed before injection (0 h) and at different post-injection timepoints. The TR channel was collected from an emission filter of 620 nm under 580 nm excitation. The Cy5.5 channel was collected from the emission filter of 710 nm under a 660 nm excitation. The body weight was recorded every other day. At Day 14, the tumors, hearts, kidneys, spleens, lungs, and livers were dissected from the euthanized mice, fixed with paraformaldehyde solution (4%), embedded in paraffin blocks, sliced into sections, stained with H&E and imaged with an optical microscope (Olympus BX51, Japan). The tumor slices were also performed TUNEL assay and CLSM imaging of the DAPI and FITC channels, which were respectively collected from the emission signal between 430 and 500 nm or 505 and 575 nm under a 405 nm or 495 nm excitation. The glycans on the tumor slices were detected following a previous method.[17, 40] The tumor tissue slices embedded in paraffin from the 8 groups of mice were dewaxed, hydrated, blocked, washed, stained with Cy3-SNA and DAPI, sealed and imaged by CLSM, which was respectively collected from the emission signal between 430 and 500 nm under a 405 nm excitation for DAPI, and 555 and 640 nm under a 543 nm excitation for Cy3.

Detection of intratumoral ATP level: After drug administration, the mice were euthanized and promptly

dissected out the intact tumor tissue, which were cut into small pieces and placed in a centrifuge tube with 70 μm filter mesh. After centrifugation at 1500 rpm for 25 min, the tumor interstitial fluid was collected. The ATP levels were measured according to the manufacturer's instructions of the ATP Chemiluminescence Assay Kit. The ATP concentrations were normalized to the tissue weight (ATP concentration/tissue weight).

ACKNOWLEDGEMENTS

This work was supported by the National Natural Science Foundation of China (22474057, 82503538) and the program B for Outstanding PhD candidate of Nanjing University.

CONFLICT OF INTEREST STATEMENT

Huangxian Ju is an editorial board member of this journal and was not involved in the editorial review or the decision to publish this article. The authors declare no conflicts of interest.

DATA AVAILABILITY STATEMENT

The data that support the findings of this study are available from the corresponding author upon reasonable request.

ETHICS STATEMENT

The animal experiments were performed according to the NIH guidelines for the care and use of laboratory animals (NIH Publication No. 85-23 Rev. 1985) and approved by Jiangsu Administration of Experimental Animals with the Certificate No. IACUC-2312006.

REFERENCES

1. A. B. Keener, *Nat. Med.* **2015**, *21*, 207.
2. R. S. Riley, C. H. June, R. Langer, M. J. Mitchell, *Nat. Rev. Drug Discovery* **2019**, *18*, 175.
3. M. G. Morvan, L. L. Lanier, *Nat. Rev. Cancer* **2016**, *16*, 7.
4. H. Xiao, E. C. Woods, P. Vukojicic, C. R. Bertozzi, *Proc. Natl. Acad. Sci. U. S. A.* **2016**, *113*, 10304.
5. P. R. Crocker, J. C. Paulson, A. Varki, *Nat. Rev. Immunol.* **2007**, *7*, 255.
6. N. Shimasaki, A. Jain, D. Campana, *Nat. Rev. Drug Discovery* **2020**, *19*, 200.
7. M. Cohen, M. Elkabets, M. Perlmutter, A. Porgador, E. Voronov, R. N. Apte, R. G. Lichtenstein, *J. Immunol.* **2010**, *185*, 5869.
8. N. M. Varki, A. Varki, *Lab. Invest.* **2007**, *87*, 851.
9. J. E. Hudak, S. M. Canham, C. R. Bertozzi, *Nat. Chem. Biol.* **2014**, *10*, 69.
10. C. Büll, M. A. Stoel, M. H. den Brok, G. J. Adema, *Cancer Res.* **2014**, *74*, 3199.
11. S. Z. Liu, V. Galat, Y. Galat, Y. K. A. Lee, D. Wainwright, J. Wu, *J. Hematol. Oncol.* **2021**, *14*, 7.
12. J. Lieberman, *Nat. Rev. Immunol.* **2003**, *3*, 361.
13. J. A. Trapani, M. J. Smyth, *Nat. Rev. Immunol.* **2002**, *2*, 735.
14. C. Bull, T. J. Boltje, N. Balneger, S. M. Weischer, M. Wassink, J. J. van Gemst, V. R. Bloemendal, L. Boon, J. van der Vlag, T. Heise, M. H. den Brok, G. J. Adema, *Cancer Res.* **2018**, *78*, 3574.
15. M. A. Gray, M. A. Stanczak, N. R. Mantuano, H. Xiao, J. F. A. Pijnenborg, S. A. Malaker, C. L. Miller, P. A. Weidenbacher, J. T. Tanzo, G. Ahn, E. C. Woods, H. Läubli, C. R. Bertozzi, *Nat. Chem. Biol.* **2020**, *16*, 1376.
16. M. Y. Xiong, G. Z. Kong, Q. Liu, L. Liu, Y. Yin, Y. Liu, H. Yuan, X. B. Zhang, W. H. Tan, *Nano Lett.* **2023**, *23*, 183.
17. Y, J. Yang, Y. R. Wang, Z. C. Chao, Y. H. Yang, Y. Y. Fang, Y. Liu, L. Ding, Y. L. Chen, H. X. Ju, *Adv. Sci.* **2024**, *11*, 2304971.
18. K. A. Browne, E. Blink, V. R. Sutton, C. J. Froelich, D. A. Jans, J. A. Trapani, *Mol. Cell Biol.* **1999**, *19*, 8604.
19. F. Rossi, N. Fredericks, A. Snowden, M. J. Allegrezza, U. Y. Moreno-Nieves, *Front. Immunol.* **2022**, *13*, 886429.
20. A. Bashiri Dezfouli, M. Yazdi, A. G. Pockley, M. Khosravi, S. Kobold, E. Wagner, G. Multhoff, *Cells* **2021**, *10*, 3390.
21. H. K. Li, C. W. Hsiao, S. H. Yang, H. P. Yang, T. S. Wu, C. Y. Lee, Y. L. Lin, J. Pan, Z. F. Cheng, Y. D. Lai, S. C. Hsiao, S. W. Tang, *Cancers* **2021**, *13*, 2724.
22. S. L. Hong, C. H. Yu, P. Wang, Y. J. Shi, W. Q. Cao, B. Cheng, D. G. Chapla, Y. H. Ma, J. Li, E. Rodrigues, Y. Narimatsu, J. R. Yates, III, X. Chen, H. Clausen, K. W. Moremen, M. S. Macauley, J. C. Paulson, P. Wu, *Angew. Chem., Int. Ed.* **2021**, *60*, 3603.
23. D. Zhang, Y. S. Zheng, Z. G. Lin, X. L. Liu, J. Li, H. H. Yang, W. H. Tan, *Angew. Chem., Int. Ed.* **2020**, *59*, 12022.
24. E. Yaghoobi, S. Shojaee, M. Ramezani, M. Alibolandi, F. Charbgoo, M. A. Nameghi, F. Khatami, M. S. Ashjaei, K. Abnous, S. M. Taghdisi, *J. Drug Delivery Sci. Technol.* **2021**, *63*, 102521.
25. G. Y. Hao, Z. P. Xu, L. Li, *RSC Adv.* **2018**, *8*, 22182.
26. M. J. Velásquez-Hernández, E. Astria, S. Winkler, W. B. Liang, H. Wiltsche, A. Poddar, R. Shukla, G. Prestwich, J. Paderi, P. Salcedo-Abraira, H. Amenitsch, P. Horcajada, C. J. Doonan, P. Falcaro, *Chem. Sci.* **2020**, *11*, 10835.
27. A. Nguyen, A. Ramesh, S. Kumar, D. Nandi, A. Brouillard, A. Wells, L. Pobezinsky, B. Osborne, A. A. Kulkarni, *Sci. Adv.* **2020**, *6*, eabc2777.
28. J. I. Scott, L. Mendive-Tapia, D. Gordon, N. D. Barth, E. J. Thompson, Z. M. Cheng, D. Taggart, T. Kitamura, A. Bravo-Blas, E. W. Roberts, J. Juarez-Jimenez, J. Michel, B. Piet, I. J. de Vries, M. Verdoes, J. Dawson, N. O. Carragher, R. A. O. Connor, A. R. Akram, M. Frame, A. Serrels, M. Vendrell, *Nat. Commun.* **2022**, *13*, 2366.
29. J. I. Scott, S. Gutkin, O. Green, Emily J. Thompson, T. Kitamura, D. Shabat, M. Vendrell, *Angew. Chem., Int. Ed.* **2021**, *60*, 5699.
30. M. Chen, K. X. Zhou, S. Y. Dai, S. Tadepalli, P. B. Balakrishnan, J. H. Xie, F. E. I. Rami, T. Dai, L. Y. Cui, J. Idoyaga, J. H. Rao, *Cell Chem. Biol.* **2022**, *29*, 1556.
31. X. Q. Li, D. Luo, J. Song, Y. L. Jia, J. Song, H. Y. Chen, J. J. Xu, *Chem. Commun.* **2022**, *58*, 8210.
32. Z. Di, J. Zhao, H. Q. Chu, W. T. Xue, Y. L. Zhao, L. L. Li, *Adv. Mater.* **2019**, *31*, 1901885.
33. E. M. Sletten, C. R. Bertozzi, *Angew. Chem., Int. Ed.* **2009**, *48*, 6974.

34. N. Shibuya, I. J. Goldstein, W. F. Broekaertg, M. Nsimba-Lubaki, B. Peetersll, W. J. Peumansg, *J. Biol. Chem.* **1987**, *262*, 1596.
35. J. A. Lopez, M. R. Jenkins, J. A. Rudd-Schmidt, A. J. Brennan, J. C. Danne, S. I. Mannering, J. A. Trapani, I. Voskoboinik, *J. Immunol.* **2013**, *191*, 2328.
36. L. M. Wang, G. J. Liu, Y. X. Ren, Y. H. Feng, X. Y. Zhao, Y. Q. Zhu, M. Chen, F. W. Zhu, Q. Liu, X. Q. Chen, *Anal. Chem.* **2020**, *92*, 14259.
37. W. B. Liang, H. S. Xu, F. Carraro, N. K. Maddigan, Q. W. Li, S. G. Bell, D. M. Huang, A. Tarzia, M. B. Solomon, H. Amenitsch, L. Vaccari, C. J. Sumby, P. Falcaro, C. J. Doonan, *J. Am. Chem. Soc.* **2019**, *141*, 2348.
38. X. L. Li, Y. L. He, L. Yang, Z. M. He, J. J. Zhu, *Chem. Commun.* **2021**, *57*, 6776.
39. L. Ye, D. L. Hermanson, B. S. Moriarity, D. S. Kaufman, *Cell Stem Cell* **2018**, *23*, 181.
40. X. F. Yu, H. F. Shi, Y. R. Li, Y. N. Guo, P. W. Zhang, G. Y. Wang, L. Li, X. Chen, L. Ding, H. X. Ju, *ACS Appl. Mater. Interfaces* **2020**, *12*, 54387.

SUPPORTING INFORMATION

Additional supporting information can be found online in the Supporting Information section at the end of this article.

How to cite this article: Y. Yang, Y. Wang, X. Li, C. Yang, Y. Yang, Y. Fang, L. Ding, Y. Chen, H. Ju, *BMEMat* **2026**, e70079. https://doi.org/10.1002/bmm2.70079